Research Article GU J Sci 39(3): 1705-1717 (2026) DOI: 10.35378/gujs.1886026

Gazi University

Journal of Science

http://dergipark.org.tr/gujs

Significant Improvement in Light Harvesting Efficiency of Naphthalene Imide Derivative Dyes via Linker Engineering for p-type Dye-Sensitized Solar Cells

Emre Burak YURDAKUL[1], Abdullah YILDIZ[2], Sule Erten ELA[3], Yusuf ERDOGDU[4,*]

[1]*Department of Physics, Institute of Science, Gazi University, 06500 Teknikokullar, Ankara, Türkiye*
[2]*Department of Energy Systems Engineering, Faculty of Engineering and Natural Sciences, Ankara Yildirim Beyazıt University, 06010 Ankara, Türkiye*
[3]*Solar Energy Institute, Ege University, Bornava-Izmir 35100, Türkiye*
[4]*Department of Physics, Faculty of Science, Gazi University, 06500 Teknikokullar, Ankara, Türkiye*

Highlights

- The performance dye was created using carbazole, naphthalene imide, and other linkers.
- Furan moiety inclusion improved key thermodynamic descriptors related to p-DSSC performance.
- Results highlight molecular orbital alignment and linker effects on dye efficiency.
- The study provides data to improve DSSC technology by explaining the influence of some parameters.

Article Info

Received:19 Feb 2026
Accepted: 9 July 2026

Keywords

P-Dssc
Dft
Homo
Lumo
Naphthalene imide

Abstract

A set of carbazole–naphthalene imide dyes with various linkers (phenyl, thiophene, furan) was designed and theoretically examined. The electronic structures, absorbance characteristics, and free-energy parameters, including hole injection (ΔG^{inject}), dye regeneration (ΔG^{reg}), and charge recombination (ΔG^{CR}), were calculated. The furan-linked dye-3 displayed the most equilibrated profile of the investigated dyes, integrating a red-shifted absorption spectrum with advantageous ΔG^{reg} and ΔG^{CR} values. These findings emphasize linker engineering as a viable design approach to enhance orbital alignment, increase light-harvesting efficiency, and mitigate recombination in *p*-DSSCs, while also indicating the necessity for subsequent experimental verification. All computations were implemented utilizing Density Functional Theory (DFT) and Time-Dependent DFT (TD-DFT) with Gaussian 09 software. Geometries were optimized employing the conductor-like polarizable continuum model (C-PCM) with chlorobenzene as the solvent at the B3LYP/6-311G(d,p) theoretical level. Molecular orbitals, absorbance spectra, ionization potentials, electron affinities, reorganization energies, and thermodynamic driving forces (ΔG^{inject}, ΔG^{reg}, ΔG^{CR}) were obtained from these computations to elucidate structure–property correlations related to *p*-DSSCs functionality.

1. INTRODUCTION

Since Grätzel's work in 1991, dye-sensitized solar cells (DSSCs) have gained interest as economical and sustainable alternatives to traditional silicon-based photovoltaics [1]. N-type DSSCs (*n*-DSSCs) using a TiO_2 photoanode have achieved power conversion efficiencies (PCE) exceeding 13% due to advancements in organic dyes with strong molar extinction coefficients and changeable donor-acceptor architectures [2,3]. Although organically synthesized, natural dyes exhibit reduced efficiencies due to their poor stability and weak binding to TiO_2 [4-6]. On the contrary, *p*-DSSCs exhibit lower efficiency than their n-type counterparts. Although considerable developments have occurred in *n*-DSSCs, developing efficient *p*-DSSCs has been limited. The lower efficiency of *p*-DSSCs arises from slow hole injection from the dye to the valence band of NiO, rapid charge recombination at the photocathode-electrolyte interface, and the absence of adequate *p*-dyes with appropriately allied orbitals [7-10].

* Corresponding author, e-mail: yerdogdu@gazi.edu.tr

Several strategies are being investigated to eliminate the insufficient efficiency problem in *p*-DSSCs, including dye design, linker engineering to enhance ICT, integration of redox mediators, and surface modification of NiO. Recent research on p-type dye-sensitized solar cells (*p*-DSSCs) has largely focused on evaluating individual sensitizers, while broader structure–property relationships remain relatively underexplored. Although several donor frameworks, including carbazole, triphenylamine, perylene, and naphthalene imide derivatives, have been investigated, comparatively little attention has been devoted to understanding how specific structural modifications influence the overall performance of p-type sensitizers. In particular, systematic studies addressing the role of linker and anchoring units are still scarce. As a result, the molecular design principles governing the optimization of p-dyes have not yet been fully established, highlighting the need for further theoretical investigations in this area. Among the molecular motifs proposed for p-DSSCs, carbazole, triphenylamine, perylene, and naphthalene imide derivatives have emerged as promising candidates due to their favorable electronic and photophysical characteristics [7-10]. Naphthalene imides are especially attractive because of their high photochemical stability, relatively long-lived excited states, tunable optical properties, and strong light-harvesting capability. Despite these advantages, their application in *p*-DSSCs has received limited attention, with only a small number of studies examining their potential as sensitizers, most notably the work reported by Sahiner et al. [7]. Consequently, significant gaps remain in the current understanding of naphthalene imide-based p-sensitizers, particularly regarding the relationship between molecular structure and charge-transfer behavior. These unresolved questions underscore the importance of comprehensive theoretical studies to guide the future design of efficient p-type sensitizers. As examples of p-dyes, the calculation results for naphthalene imide, carbazole, and an isoindigo derivative, published by various researchers, are presented. Sahiner et al. determined the -6.11 eV to -6.10 eV (E_{HOMO}) and -3.11 to -3.06 eV (E_{LUMO}) of the naphthalene imide sensitizers. Carella et al. reported carbazole-based dyes with E_{HOMO} values of -6.06 and -5.85 eV and E_{LUMO} values of -3.28 to -2.96 eV. Ameline and colleagues investigated isoindigo derivatives with E_{HOMO} values ranging from approximately -6.0 to -5.0 eV and E_{LUMO} values ranging from approximately -3.5 to -2.75 eV.

Despite extensive work on donor–acceptor organic dyes for dye-sensitized solar cells, the role of linker units in *p*-DSSC sensitizers has not yet been systematically explored or thermodynamically focused. manner. In this study, we propose a clear linker-engineering approach for carbazole–naphthalene imide dyes, in which phenyl, thiophene, and furan bridges are selectively introduced while maintaining the donor–acceptor framework. This strategy allows the direct assessment of how the linker alone governs the optoelectronic behavior of the sensitizers. Rather than focusing solely on frontier orbital alignment or the hole-injection driving force (ΔG^{inject}), as is commonly done in previous theoretical studies, the present results suggest that dye regeneration (ΔG^{reg}) and resistance to charge recombination (ΔG^{CR}) may be influential descriptors alongside ΔG^{inject} when assessing the potential performance of p-type sensitizers. By jointly evaluating light-harvesting efficiency, reorganization energies, and thermodynamic driving forces, we identify a furan-linked dye that offers the most balanced profile, combining red-shifted absorption with efficient regeneration and suppressed recombination, despite a moderate hole-injection driving force. By systematically varying the linker unit while preserving the same carbazole–naphthalene imide backbone, we demonstrate that energy-level alignment with the NiO valence band and the I^-/I_3^- redox couple can be finely tuned without altering the chromophoric core. The molecular design adopted here prioritizes favorable ΔG^{reg} and ΔG^{CR} values, accepting a modest reduction in ΔG^{inject}, which generally occurs on ultrafast timescales and may not always represent the rate-limiting step in *p*-DSSCs. At the same time, the use of conjugated and heteroaromatic linkers extends π-conjugation across the donor–linker–acceptor framework, strengthens intramolecular charge transfer, and enhances visible-light absorption.

Recent studies have demonstrated that naphthalene imide derivatives constitute a versatile class of electron-accepting units for *p*-DSSCs owing to their strong electron-withdrawing character, tunable electronic properties, and favorable charge-separation characteristics. At the same time, research on NiO-based photocathodes and donor–acceptor organic sensitizers have expanded considerably, providing valuable insights into how molecular structure influences charge-transfer processes and recombination behavior in *p*-DSSCs [11-16]. This work presents one of the most systematic theoretical evaluations of linker-dependent energetics in naphthalene imide-based p-sensitizers, providing clear structure–property relationships that move beyond molecule-specific observations. The results establish linker engineering as

a rational design principle for improving *p*-type and tandem DSSC sensitizers and offer practical guidance for future experimental validation.

2. COMPUTATIONAL DETAILS

A DFT-based computational procedure was utilized to investigate the electronic structures and photovoltaic descriptors outlined below. All theoretical computations are achieved with the Gaussian 09 software [17]. The DFT method uses the B3LYP/6-311 G(d,p) level of theory [18-20]. The geometric optimizations were conducted using the C-PCM model with chlorobenzene solvent without symmetry constraints [2,3]. Subsequent frequency analysis demonstrated that the structures represent local minima on the potential energy surface. The molecular structures and molecular orbitals of the designed dyes were obtained using the GaussView 5 software package [21]. Additionally, to predict spectral characteristics, electronic excitation energies were calculated using TD-DFT.

The B3LYP functional with the 6-311G(d,p) [20] basis set was employed for all calculations. This choice also ensures direct comparability with the work of Sahiner et al., who investigated structurally analogous naphthalene imide *p*-dyes at the same theoretical level [7]. Although long-range corrected functionals such as CAM-B3LYP are often recommended for charge-transfer excitations, B3LYP has been widely employed for structurally related p-DSSC sensitizers and provides a reliable framework for comparative trend analysis. Since the primary objective of the present work is to investigate the relative influence of linker modification within a homologous dye series, methodological consistency with previous studies was considered particularly important. Using B3LYP in chlorobenzene thus guarantees methodological consistency and allows reliable benchmarking of ΔE_{gap}, HOMO/LUMO alignment, and spectral properties against previously reported experimental and theoretical data.

The power conversion efficiency (η) of DSSCs is given by Equation (1):

$$\eta = FF\frac{V_{OC}\,J_{SC}}{P_{inc}}\,. \tag{1}$$

Various variables can affect the operation of DSSCs, notably the power conversion efficiency (η), which is contingent upon multiple factors, including V_{OC}, J_{SC}, FF, and P_{inc} values. V_{OC} denotes the open-circuit photovoltage, J_{SC} represents the short-circuit current density, FF signifies the fill factor, and P_{inc} indicates the incident solar power

$$J_{SC} = \int LHE(\lambda)\phi_{inject}\eta_{collect}d\lambda\,. \tag{2}$$

LHE(λ) signifies the light-harvesting efficiency at a specific wavelength, ϕ_{inject} represents the electron injection efficiency, and $\eta_{collect}$ indicates the charge-collection efficiency. The $\Delta G^{inject,}$ ΔG^{CZ}, ΔG^{reg}, and LHE were the critical influencing elements on J_{SC}. Therefore, these parameters are the essential factors affecting the performance of DSSC devices [22, 23].

3. RESULTS AND DISCUSSION

Figure 1 shows the dye compounds examined. Dye-1 denotes a molecule where the anchor unit is directly linked to the donor unit. By introducing thiophene (dye-2), furan (dye-3), and phenyl (dye-4) molecules between the donor unit and anchor unit, three new molecules are obtained from dye-1. Consequently, four distinct molecules are created by connecting different units between the donor and anchor units. The first phase of this research involved performing a conformer analysis of the dye compounds through the Spartan 14 software package [24]. This conformational analysis was executed using the Merck Molecular Force Field (MMFF) within a molecular mechanics framework. Previous studies [25] have comprehensively described the procedural steps undertaken during the conformer analysis.

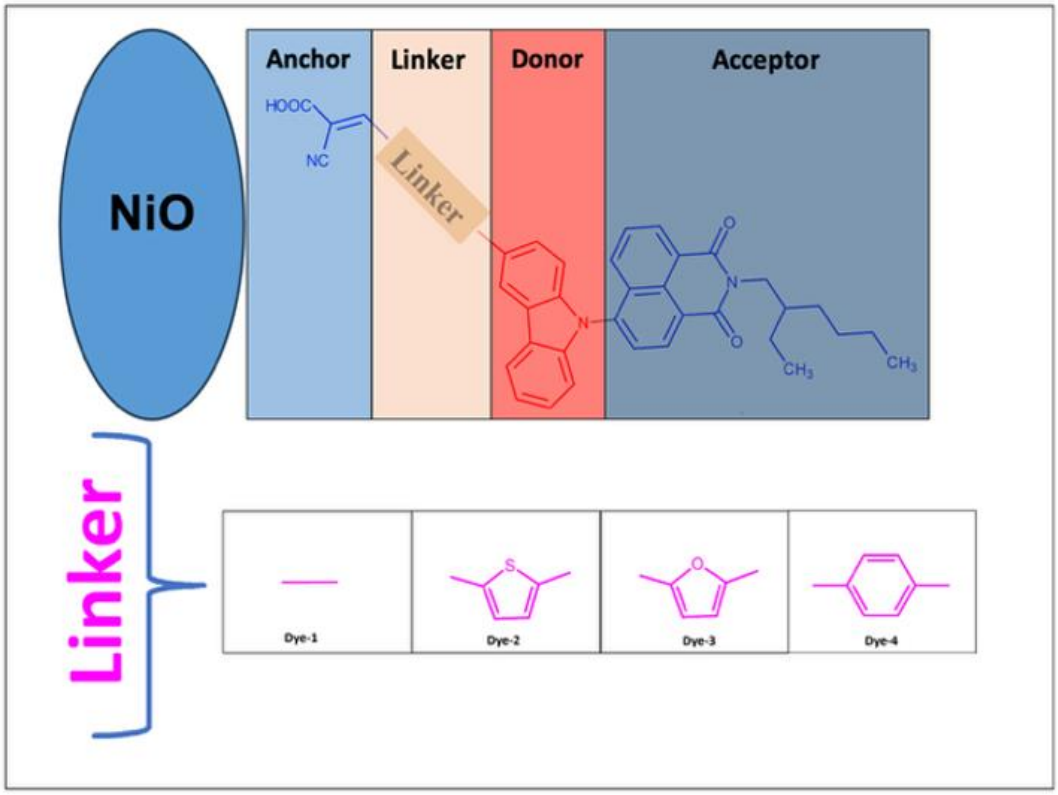


Figure 1. *Chemical structures of the designed carbazole–naphthalene imide dyes*

3.1. HOMO-LUMO of the Designed Dyes

Figure 2 shows the alignment of the HOMO and LUMO energy levels of the designed dyes relative to the valence band of NiO (≈ –5.0 eV) and the redox potential of the electrolyte (≈ –4.8 eV). Such alignment is crucial for assessing the thermodynamic feasibility of hole injection and dye regeneration in *p*-DSSCs. For efficient operation of p-type dye-sensitized solar cells, the energy levels of the sensitizer must be appropriately aligned with both the NiO photocathode and the electrolyte. In general, the HOMO should be located below the valence band edge of NiO to enable hole injection, while the energetic position of the excited dye state must allow subsequent regeneration by the redox mediator. Among the investigated structures, dye-3 presents a particularly favorable arrangement of frontier orbital energies, with a HOMO level of −5.79 eV and a LUMO level of −2.91 eV.

Changes introduced through the linker units are reflected in the dyes' electronic structure. The incorporation of thiophene, furan, and phenyl bridges alters the extent of intramolecular charge transfer and influences the optical response of the molecules. As shown in Table 1, dye-3 exhibits the smallest HOMO–LUMO separation (2.88 eV), slightly lower than that of dye-2 (2.94 eV). This trend is consistent with the redshift observed in the absorption spectra and the corresponding increase in the calculated light-harvesting efficiency. The calculated frontier orbital energies of all four dyes fall within the range commonly reported for functional p-type DSSC sensitizers. While the differences among the molecules are not dramatic, the furan-containing dye-3 combines a relatively elevated HOMO level with a narrow band gap and favorable absorption characteristics. When these observations are considered together with the thermodynamic descriptors summarized in Tables 2 and 4, dye-3 emerges as the most balanced member of the series. Although further experimental and interfacial studies are required to verify these predictions, the present results suggest that the furan linker may be a useful structural element for developing new naphthalene imide-based p-type sensitizers.

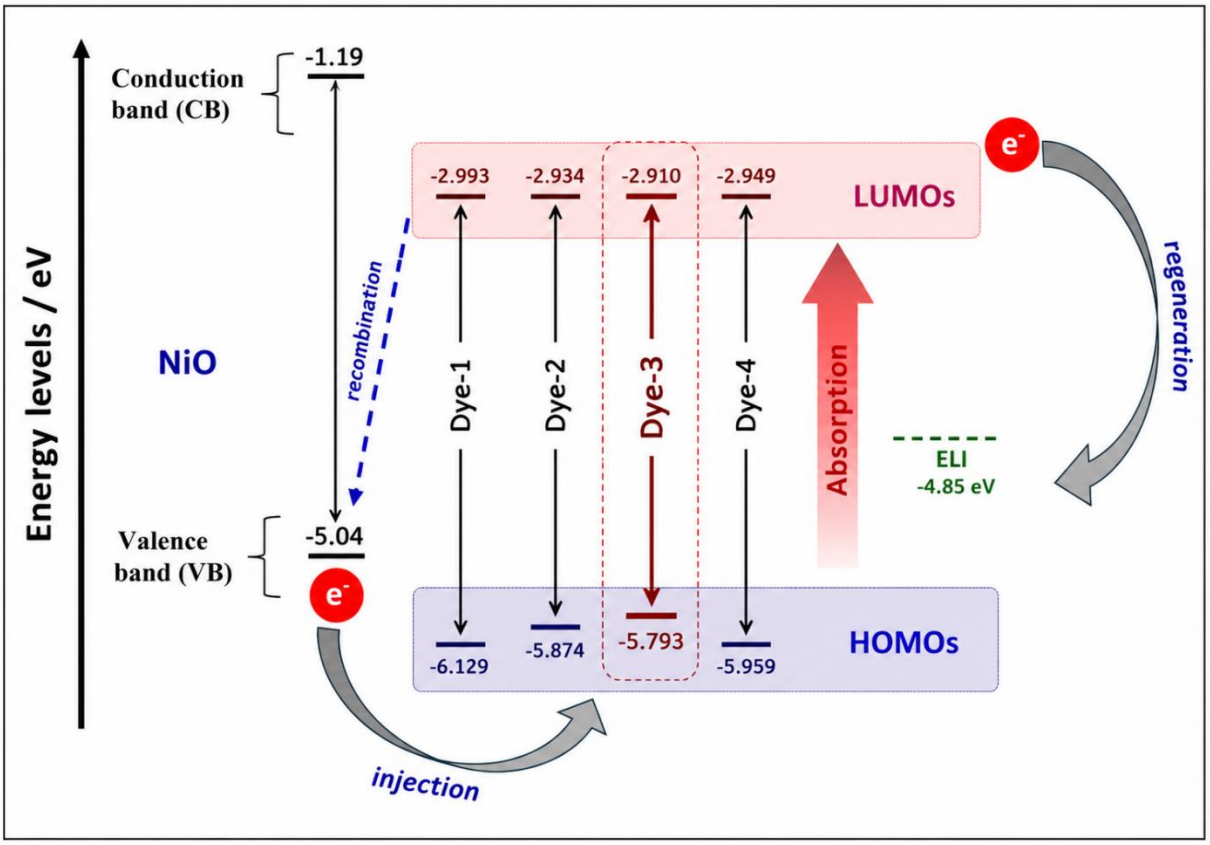


Figure 2. *HOMO–LUMO energy alignment of the designed dyes relative to the NiO valence band (≈ –5.0 eV) and the I^-/I_3^- redox potential (≈ –4.8 eV)*

Table 1. *Calculated frontier orbital energies (E_{HOMO}, E_{LUMO}) and energy gaps (E_{gap}) of the designed carbazole–naphthalene imide dyes*

	E_{HOMO} (eV)	E_{LUMO} (eV)	ΔE_{gap} (eV)
Dye-1	-6.12	-2.99	3.13
Dye-2	-5.87	-2.93	2.94
Dye-3	-5.79	-2.91	2.88
Dye-4	-5.95	-2.94	3.01
Sahiner et al. [7]	-6.11 to -6.10	-3.05 to -3.11	3.05 to 2.99
Ameline et al. [10]	-6.0 to -5.0	-3.5 to -2.75	
Carella et al. [8]	-6.06 to -5.85	-3.28 to -2.96	

Figure 3 depicts the frontier molecular orbitals of the designed dyes. The HOMO and HOMO–1 orbitals are primarily localized over the donor and linker regions, supporting effective hole transfer toward the NiO valence band. In contrast, the LUMO and LUMO+1 orbitals are distributed along the linker and partially over the anchoring unit, thereby providing a pathway for electron-density delocalization and efficient dye regeneration with the I^-/I_3^- electrolyte. The observed orbital distributions and energy alignments collectively confirm that the designed naphthalene imide-based dyes are thermodynamically suitable for *p*-DSSC applications. The HOMO distribution over the donor and linker units is particularly important for p-DSSCs because hole injection from the excited dye into the NiO valence band is the dominant charge-transfer process. The LUMO distribution remains relevant for excited-state charge separation and dye regeneration; however, its role should be interpreted within the context of p-type operation rather than direct electron injection into a semiconductor.

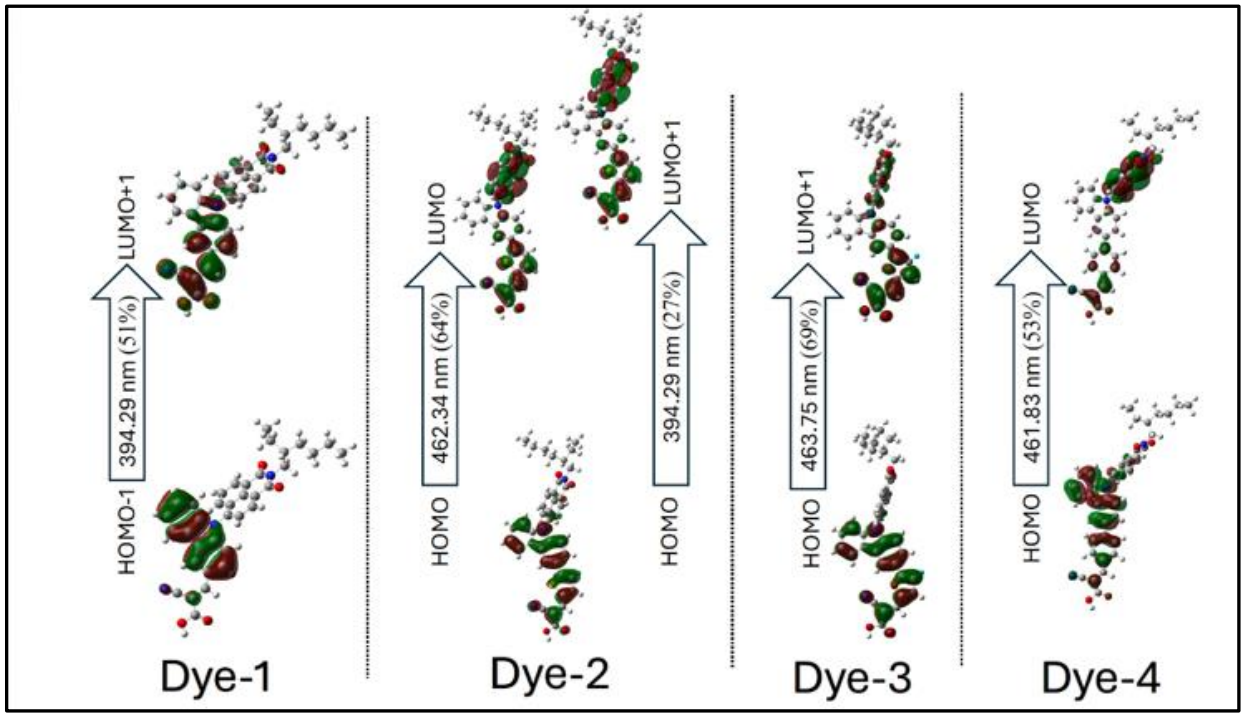


Figure 3. *Frontier molecular orbital distributions (HOMO, HOMO–1, LUMO, LUMO+1) of the designed dyes*

3.2. Optoelectronic Properties

ΔG^{inject}, ΔG^{reg}, and ΔG^{CR} play crucial roles in the performance of *p*-DSSCs. These energetic parameters influence the efficiency of charge transfer processes within the cell. The parameters ΔG^{inject}, ΔG^{reg}, and ΔG^{CR} represent the free energy changes associated with three key processes in *p*-DSSCs: hole injection from the photoexcited dye into the valence band of the semiconductor, dye regeneration by the redox couple, and charge recombination between the oxidized dye and the reduced electrolyte species, respectively. The calculated values of LHE, ΔG^{inject}, ΔG^{reg}, and ΔG^{CR} for the designed dyes are summarized in Table 2. A more negative hole injection free energy promotes efficient hole injection from the photoexcited dye into the semiconductor. This process is essential for initiating charge separation and generating current in *p*-DSSCs. Dye regeneration free energy is associated with the energy difference between the oxidized dye and the redox mediator. A more negative dye regeneration free energy facilitates the reduction of the oxidized dye by the redox mediator, restoring the dye to its ground state. Efficient dye regeneration is crucial for maintaining continuous solar cell operation and preventing unwanted charge recombination. Negative values of ΔG^{inject} and ΔG^{reg} indicate thermodynamically favorable processes, where a more negative ΔG^{inject} corresponds to faster hole injection and a more negative ΔG^{reg} reflects more efficient dye regeneration. Within the sign convention adopted in this work, larger positive ΔG^{CR} values indicate a thermodynamically less favorable charge recombination process. However, actual recombination rates are also influenced by kinetic factors, electronic coupling, and interfacial interactions, and therefore, ΔG^{CR} should be interpreted as a thermodynamic descriptor rather than a direct measure of recombination kinetics. Although a more negative ΔG^{reg} generally favors dye regeneration, excessively large regeneration driving forces may also introduce additional energy losses. Therefore, ΔG^{reg} should not be optimized independently but rather considered alongside charge recombination, light-harvesting efficiency, and other photovoltaic descriptors. In the present study, the favorable performance of dye-3 is attributed to its balanced combination of ΔG^{reg}, ΔG^{CR}, and optoelectronic properties rather than to its regeneration driving force alone. Consequently, the superior characteristics of dye-3 should not be attributed solely to its more negative ΔG^{reg} value but rather to the combined effect of favorable regeneration, recombination resistance, and charge-transport properties.

Table 2. *Key optoelectronic descriptors of the designed dyes*

	Dye-1	Dye-2	Dye-3	Dye-4
LHE	0.53	0.79	0.77	0.79
ΔG^{inject}	-1.08	-0.83	-0.75	-0.91
ΔG^{reg}	-1.85	-1.91	-1.94	-1.90
ΔG^{CR}	2.04	2.10	2.13	2.09

Among them, dye-1 shows the most favorable ΔG^{inject}, indicating the most potent driving force for hole injection. However, introducing linkers such as furan, thiophene, and phenyl reduces the hole injection driving force compared to dye-1. Including furan, thiophene, and phenyl linker units into dye-1 reduces hole injection efficiency. In contrast to the ΔG^{inject} parameter, the ΔG^{reg} and ΔG^{CR} parameters indicate that dye-1 has reduced dye regeneration and charge recombination efficiency to the other dyes. The ΔG^{CR} and ΔG^{reg} analyses showed significant differences in the efficiency driving forces of the dyes studied. Dye-3 possesses the most favorable characteristics, demonstrating enhanced driving forces for dye regeneration and increased resistance to charge recombination relative to other dyes. The equilibrium between efficient dye regeneration and low charge recombination is essential for the performance of *p*-DSSCs, as this equilibrium directly influences the stability and efficiency of the devices. The elevated ΔG^{CR} and ΔG^{reg} values of dye-3 suggest a greater resistance to charge recombination and more efficient dye regeneration, indicating favorable thermodynamic characteristics for p-DSSC applications. Despite dye-3 exhibiting reduced hole injection efficiency relative to other dyes (notably dye-1), its elevated ΔG^{reg}, and ΔG^{CR} values provide greater force, as evidenced by the experimental work conducted by Sen et al. [23]. Given that hole injection occurs rapidly, the slower processes of dye regeneration and charge recombination are more critical determinants of the driving force of the dye [23]. Since ΔG^{inject} in p-DSSCs generally occurs on ultrafast timescales, it may not always represent the rate-limiting step in device operation. In contrast, dye regeneration and recombination processes can also play important roles in determining the overall charge-transfer behavior of the device. Consequently, dyes that exhibit favorable ΔG^{reg} and ΔG^{CR} values may provide advantageous thermodynamic conditions for charge separation and reduced recombination losses in p-DSSC systems.

The energetic driving forces provide a more quantitative lens to assess the relative suitability of each dye. For instance, dye-3 exhibits $\Delta G^{reg} = -1.94$ eV and $\Delta G^{CR} = 2.13$ eV, which are both more favorable than typical carbazole derivatives reported by Carella et al. ($\Delta G^{reg} \approx -1.7$ to 1.8 eV) [8] and the naphthalene imide values summarized by Sahiner et al. ($\Delta G^{CR} \approx 1.8$ to 2.0 eV) [7]. A more negative ΔG^{reg} generally indicates more favorable thermodynamic conditions for dye regeneration by the redox mediator. At the same time, a larger ΔG^{CR} indicates stronger resistance to charge recombination at the dye–electrolyte interface. By contrast, ΔG^{inject} values, although important, occur on ultrafast femtosecond timescales and seldom represent the performance bottleneck in *p*-DSSCs. Thus, the ΔG^{reg} and ΔG^{CR} values of dye-3 indicate favorable thermodynamic conditions for dye regeneration and suppression of charge recombination, potentially compensating for its slightly less favorable ΔG^{inject} relative to dye-1. These findings suggest that, within the framework of the present theoretical study, regeneration and recombination energetics may be as important as, or potentially more influential than, hole injection driving force in the design of efficient p-sensitizers.

The LHE data indicate that dye-2 and dye-4 obtain the maximum efficiencies (0.79%), closely followed by dye-3 (0.77%), while dye-1 exhibits the lowest value (0.53%). Despite dye-3 exhibiting a slightly smaller LHE than dye-2, it surpasses dye-1 substantially and is enhanced by its advantageous ΔG^{reg}, ΔG^{CR}, and reorganization energy parameters. A more negative ΔG^{reg} generally indicates more favorable thermodynamic conditions for dye regeneration by the redox mediator. Although the differences among the linker-containing dyes are relatively small, the increase in LHE from dye-1 (0.53) to dye-2–dye-4 (0.77–0.79) indicates that the introduction of π-linkers improves the light-harvesting ability of the dyes. Therefore, the LHE discussion was revised to avoid overemphasizing minor differences between dye-2, dye-3, and dye-4. Instead, the main emphasis was placed on the overall enhancement observed upon linker incorporation and on the combined evaluation of LHE with ΔG^{inject}, ΔG^{reg}, ΔG^{CR}, and reorganization energy parameters.

Optimizing these free energy parameters is essential for improving *p*-DSSC efficiency. Current research focuses on designing dyes, semiconductor materials, and electrolytes with precisely aligned energy levels to maximize hole injection and dye regeneration while minimizing charge recombination losses. This strategy enhances charge separation, facilitates faster charge transport, and improves carrier collection, resulting in higher photocurrents and overall device efficiency [23]. Dye-3 exhibits LHE, the most balanced driven forces, and charge recombination characteristics among the investigated dyes. These features indicate that dye-3 possesses favorable characteristics for potential application as a p-sensitizer in p-DSSCs.

3.3. Ionization Potential and Electron Affinity of the Designed Dyes

Table 3. *Ionization potential (IP), electron affinity (EA), and reorganization energy components (λ_e, λ_h, λ_{total}) of the designed dyes*

	Dye-1	Dye-2	Dye-3	Dye-4	Sahiner et al. [7]	
IP	6.22	5.82	5.77	5.94	6.11	6.10
EA	2.93	2.97	2.91	2.91	3.05	3.11
η	1.64	1.42	1.43	1.51	1.52	1.49
λ_e	0.25	0.23	0.19	0.20	NA	NA
λ_h	0.10	0.23	0.20	0.16	NA	NA
λ_{total}	0.35	0.47	0.39	0.37	NA	NA

*Taken from Ref [7]

The IP and EA provide critical insight into the optoelectronic behavior of the designed dyes. IP reflects the tendency of a dye to donate a hole, while EA indicates its ability to accept an electron. Lower IP values favor hole injection, whereas higher EA values contribute to excited-state stabilization and enhanced charge transfer in *p*-DSSCs [26, 27]. As summarized in Table 3, dye-3 exhibits the lowest IP (5.77 eV), suggesting superior hole injection capability compared to the other dyes. On the other hand, dye-1 shows the highest IP (6.22 eV), indicating greater resistance to electron loss and enhanced essential stability. Dye-2 has the highest EA (2.97 eV), implying a stronger ability to accept electrons upon photoexcitation. When comparing the EA value of dye-3 with that of dye-2, the difference was 0.06 eV.

Examining the reorganization energy indicates that dye-3 may have superior charge transport capabilities. Although dye-2 possesses the highest total reorganization energy (0.47 eV), dye-3 demonstrates a more equilibrated profile with intermediate λ_e (0.19 eV) and λ_h (0.20 eV) values. Dye-3 exhibits a reduced overall reorganization energy of 0.39 eV compared to dye-2. This indicates that dye-3 may enhance effective hole transport while preserving appropriate electron transfer characteristics. Reduced reorganization energies are typically linked to enhanced charge mobility.

3.4. Absorption Spectroscopy

TD-DFT calculations were used to assess how furan, thiophene, and phenyl linkers affect absorption. Table 2 summarizes the calculated λmax values, oscillator strengths (*f*), and main transition types for each dye. Figure 4 shows the theoretical UV-vis spectra.

The simulated UV–Vis spectra, TD-DFT configurations, and orbital maps reveal clear ICT features beyond the numerical listing of λmax and oscillator strengths. As tabulated in Table 4, the main excitations of the linker-containing dyes are dominated by HOMO→LUMO and HOMO→LUMO+1 transitions (dye-2: HOMO→LUMO+1, 64%; dye-3: HOMO→LUMO+1, 69%; dye-4: HOMO→LUMO, 53%), whereas dye-1 is characterized by a less delocalized HOMO-1→LUMO+1 transition (51%). This accounts for the much weaker oscillator strength of dye-1 ($f = 0.33$) compared to the higher values of dyes 2 and 4 ($f \approx 0.68$).

Table 4. *Simulated UV–vis spectral data (excitation energies (E_{ex}), maximum absorption wavelengths (λ_{max}), oscillator strengths (f), and main orbital transition configurations) of the dyes*

Dye	E_{ex} (eV)	λ_{max} (nm)	*f*	main configuration
Dye-1	3.14	394.29	0.33	HOMO-1→LUMO+1 (51%)
Dye-2	2.68	462.34	0.67	HOMO→LUMO+1 (64%); HOMO→LUMO (27%)
Dye-3	2.67	463.75	0.63	HOMO→LUMO+1 (69%)
Dye-4	2.68	461.83	0.68	HOMO→LUMO (53%)
Sahiner et al. [7]	2.55	484.74	0.30	HOMO→LUMO (95%), HOMO→LUMO+1 (3%)
	2.52	491.32	0.35	HOMO→LUMO (94%); HOMO→LUMO+1 (3%)

The frontier orbital distributions further support these spectral trends. In dyes 2 and 4, the HOMO is delocalized across both the carbazole donor and the π-linker, while the LUMO extends toward the naphthalene imide acceptor and anchoring group. This spatial separation enhances the transition dipole moment and strengthens ICT, explaining their higher oscillator strengths and red-shifted absorption. In contrast, dye-1 shows a more localized HOMO-LUMO transition with limited delocalization, resulting in reduced ICT efficiency. Dye-3, although exhibiting a slightly lower oscillator strength (f = 0.64) than dyes 2 and 4, combines its robust ICT character with more favorable ΔG^{reg} and ΔG^{CR} values. Dye-3 can more effectively exploit absorbed photons by suppressing charge recombination, leading to a more balanced photovoltaic profile.

Overall, these results emphasize that oscillator strength alone is not a sufficient predictor of photovoltaic performance. Strong ICT, arising from donor-to-acceptor delocalization across the π-bridge, does enhance absorption and red-shifts the spectra, but optimal sensitizers must also exhibit favorable regeneration and recombination energetics. The interplay between orbital topology (Figure 3), transition character (Table 4), and thermodynamic parameters (Table 2) explains why the furan-linked dye-3 emerges as the most promising candidate among the designed sensitizers. Finally, it should be noted that the present analysis is limited to gas-phase and implicit-solvent models. Explicit modeling of dye adsorption on NiO and interfacial charge-transfer processes would provide deeper insight into realistic device operation and should be addressed in future work.

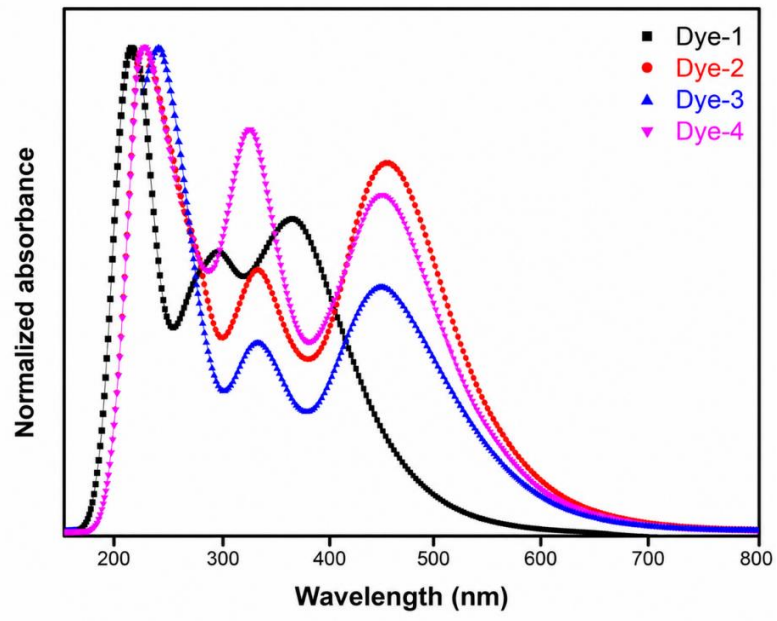


Figure 4. *Simulated UV–Vis absorption spectra of the designed dyes (B3LYP/6-311G(d,p), CPCM, chlorobenzene)*

4. CONCLUSIONS

This study systematically explored carbazole–naphthalene imide dyes with various linkers to evaluate how well they function as *p*-dyes in DSSCs. DFT and TD-DFT calculations at the B3LYP/6-311G(d,p) level enabled the evaluation of key optoelectronic descriptors, including frontier orbital alignment, light-harvesting efficiency, and the thermodynamic driving forces governing hole injection, dye regeneration, and charge recombination. The results suggest that linker engineering significantly influences the optoelectronic properties of these systems. Among the four designed dyes, the furan-linked dye-3 provided the most balanced photovoltaic profile, combining a red-shifted absorption spectrum with favorable ΔG^{reg} and ΔG^{CR} values, ensuring efficient dye regeneration and enhanced resistance to recombination. Dye-3 is highlighted as a dye designed with more balanced thermodynamic and spectral properties.

Benchmarking against previously reported carbazole-, isoindigo-, and naphthalene imide-based sensitizers further highlights the advantages of dye-3, which falls within the optimal frontier orbital ranges required for NiO/I^-/I_3^- photocathodes while simultaneously improving light-harvesting efficiency and charge stabilization. These findings reinforce the importance of rational molecular design and targeted linker modification as a strategy to overcome the intrinsic challenges of *p*-DSSCs. The comparative analysis suggests that ΔG^{reg} and ΔG^{CR} may play an important role in the theoretical evaluation of p-sensitizers, alongside ΔG^{inject}, which generally occurs on ultrafast timescales and may not always be the rate-limiting step in device operation [17].

This study offers quantitative analysis of structure–property relationships in carbazole–naphthalene imide dyes, addressing gaps in the theoretical literature on *p*-DSSCs. Identifying dye-3 as a promising sensitizer underscores the potential of linker engineering as a rational design tool for next-generation *p*-sensitizers, offering guidance for future computational benchmarking and experimental validation to enhance the working of p-type and tandem DSSCs. On the other hand, these findings are based solely on theoretical calculations, and experimental validation will be essential in future studies to confirm the practical applicability of the designed dyes in *p*-DSSCs.

Despite the promising theoretical results obtained for the designed dyes, several limitations of the present study should be acknowledged. The calculations were performed using isolated dye molecules within an implicit solvent environment and therefore do not explicitly account for dye adsorption on NiO surfaces, interfacial electronic coupling, or dynamic charge-transfer processes occurring at the dye–semiconductor interface. Future studies should incorporate atomistic dye/NiO models and interfacial simulations to obtain a more realistic description of charge injection and recombination mechanisms. Furthermore, experimental synthesis and photovoltaic characterization of the proposed dyes will be essential for validating theoretical predictions and assessing their practical applicability in p-type DSSCs.

ACKNOWLEDGMENT

This work is based on the doctoral dissertation of Emre Burak YURDAKUL, Graduate School of Natural and Applied Sciences, Gazi University. The authors thank Dr. Ömer DERELİ for performing the calculations using Spartan 14 software.

DECLARATION OF ARTIFICIAL INTELLIGENCE (AI) USE

Generative AI agents or large language models (LLMs) were used only to improve clarity and quality of the English language presentation of the manuscript.

CONFLICTS OF INTEREST

No conflict of interest was declared by the authors.

REFERENCES

[1] O'Regan, B., and Grätzel, M., "A low-cost, high-efficiency solar cell based on dye-sensitized colloidal TiO2 films", Nature, 353(6346): 737-740, (1991). DOI: https://doi.org/10.1038/353737a0

[2] Akdogan, N., Ortatepe, B., Atli, A., Disli, A., Erdogdu, Y., and Yildiz, A., "A joint theoretical and experimental study on a Tetrazole-Anchored BODIPY-Based dye at the surface of TiO2 for dye-sensitized solar cell applications", Physica Status Solidi A, 221(3), (2023). DOI: https://doi.org/10.1002/pssa.202300513

[3] Akdogan, N., Alp, M., Atilgan, A., Disli, A., Erdogdu, Y., and Yildiz, A., "An AZO dye with nitril anchoring to dye-sensitized solar cell performance: A theoretical and experimental investigation", Materials Letters, 351:135075, (2023). DOI: https://doi.org/10.1016/j.matlet.2023.135075

[4] Erdogdu, M., Atilgan, A., Erdogdu, Y., and Yildiz, A., "Flavonoid from Hedera helix fruits: A promising new natural sensitizer for DSSCs", Journal of Photochemistry and Photobiology A: Chemistry, 448: 115288, (2023). DOI: https://doi.org/10.1016/j.jphotochem.2023.115288

[5] Erdogdu, M., Atilgan, A., Erdogdu, Y., and Yildiz, A., "Natural dyes extracted from Ligustrum vulgare, Juniperus sabina, and Papaver rhoeas for novel DSSC applications", Materials Letters, 358: 135811, (2023). DOI: https://doi.org/10.1016/j.matlet.2023.135811

[6] Mathew, S., Yella, A., Gao, P., Humphry-Baker, R., Curchod, B.F.E., Ashari-Astani, N., Tavernelli, I., Rothlisberger, U., Nazeeruddin, M.K., and Grätzel, M., "Dye-sensitized solar cells with 13% efficiency achieved through the molecular engineering of porphyrin sensitizers", Nature Chemistry, 6(3): 242-247, (2014). DOI: https://doi.org/10.1038/nchem.1861

[7] Sahiner, F., Ali, A.K., Denizaltı, S., Kandemir, Z., and Erten-Ela, S., "Naphthalene imides as novel p-type sensitizers for NiO-based p-type dye-sensitized solar cells", New Journal of Chemistry, 44(36): 15526-15537, (2020). DOI: https://doi.org/10.1039/d0nj03266b

[8] Carella, A., Centore, R., Borbone, F., Toscanesi, M., Trifuoggi, M., Bella, F., Gerbaldi, C., Galliano, S., Schiavo, E., Massaro, A., Muñoz-García, A.B., and Pavone, M., "Tuning optical and electronic properties in novel carbazole photosensitizers for p-type dye-sensitized solar cells", Electrochimica Acta, 292: 805-816, (2018). DOI: https://doi.org/10.1016/j.electacta.2018.09.204

[9] Zhang, T., Guan, W., Yan, L., Ma, T., Wang, J., and Su, Z., "Theoretical studies on POM-based organic–inorganic hybrids containing double D–A1–π–A2 chains for high-performance p-type dye-sensitized solar cells", Physical Chemistry Chemical Physics, 17(7): 5459-5465, (2014). DOI: https://doi.org/10.1039/c4cp04890c

[10] Ameline, D., Diring, S., Farre, Y., Pellegrin, Y., Naponiello, G., Blart, E., Charrier, B., Dini, D., Jacquemin, D., and Odobel, F., "Isoindigo derivatives for application in p-type dye sensitized solar cells", RSC Advances, 5(104): 85530-85539, (2015). DOI: https://doi.org/10.1039/c5ra11744e

[11] Marri, A.R., Flint, H., Gibson, E.A., and Fielden, J., "Pyridyl anchored indolium dyes for the p-type dye sensitized solar cell", Dyes and Pigments, 202: 110244, (2022). DOI: https://doi.org/10.1016/j.dyepig.2022.110244

[12] Muñoz-García, A.B., Benesperi, I., Boschloo, G., Concepcion, J.J., Delcamp, J.H., Gibson, E.A., and Freitag, M., et al., "Dye-sensitized solar cells strike back", Chemical Society Reviews, 50(22): 12450-12550, (2021). DOI: https://doi.org/10.1039/d0cs01336f

[13] Odobel, F., Pellegrin, Y., Gibson, E.A., Hagfeldt, A., Smeigh, A.L., and Hammarström, L., "Recent advances and future directions to optimize the performances of p-type dye-sensitized solar cells", Coordination Chemistry Reviews, 256(21–22): 2414-2423, (2012). DOI: https://doi.org/10.1016/j.ccr.2012.04.017

[14] Favereau, L., Warnan, J., Pellegrin, Y., Blart, E., Boujtita, M., Jacquemin, D., and Odobel, F., "Diketopyrrolopyrrole derivatives for efficient NiO-based dye-sensitized solar cells", Chemical Communications, 49(73): 8018-8020, (2013). DOI: https://doi.org/10.1039/c3cc44232b

[15] Keremane, K.S., Planchat, A., Pellegrin, Y., Jacquemin, D., Odobel, F., and Vasudeva Adhikari, A., "Push–Pull Phenoxazine-Based Sensitizers for p-Type DSSCs: Effect of Acceptor Units on Photovoltaic Performance", ChemSusChem, 15(16): e202200520, (2022). DOI: https://doi.org/10.1002/cssc.202200520

[16] Etefa, H.F., Kumar, V., Dejene, F.B., Efa, M.T., and Jule, L.T., "Modification of flexible electrodes for p-type (nickel oxide) dye-sensitized solar cell performance based on the cellulose nanofiber film", ACS Omega, 8(17): 15249-15258, (2023). DOI: https://doi.org/10.1021/acsomega.3c00383

[17] Frisch, M.J., Trucks, G.W., Schlegel, H.B., Scuseria, G.E., Robb, M.A., Cheeseman, J.R., Scalmani, G., Barone, V., Mennucci, B., Petersson, G.A., Nakatsuji, H., Caricato, M., Li, X., Hratchian, H.P., Izmaylov, A.F., Bloino, J., Zheng, G., Sonnenberg, J.L., Hada, M., Ehara, M., Toyota, K., Fukuda, R., Hasegawa, J., Ishida, M., Nakajima, T., Honda, Y., Kitao, O., Nakai, H., Vreven, T., Montgomery, J.A., Peralta, J.E., Ogliaro, F., Bearpark, M., Heyd, J.J., Brothers, E., Kudin, K.N., Staroverov, V.N., Kobayashi, R., Normand, J., Raghavachari, K., Rendell, P.G., Burant, J.C., Iyengar, S.S., Tomasi, J., Cossi, M., Rega, N., Millam, J.M., Klene, M., Knox, J.E., Cross, J.B., Bakken, V., Adamo, C., Jaramillo, J., Gomperts, R., Stratmann, R.E., Yazyev, O., Austin, A.J., Cammi, R., Pomelli, C., Ochterski, J.W., Martin, R.L., Morokuma, K., Zakrzewski, V.G., Voth, G. A., Salvador, P., Dannenberg, J.J., Dapprich, S., Daniels, A.D., Farkas, O., Foresman, J.B., Ortiz, J. V., Cioslowski, J., Fox, D.J., "Gaussian 09, Revision D.01", Gaussian Inc., Wallingford CT, (2009).

[18] Becke, A.D., "Density-functional thermochemistry. III. The role of exact exchange", The Journal of Chemical Physics, 98(7): 5648-5652, (1993). DOI: https://doi.org/10.1063/1.464913

[19] Lee, C., Yang, W., and Parr, R.G., "Development of the Colle-Salvetti correlation-energy formula into a functional of the electron density", Physical Review B, 37(2): 785-789, (1988). DOI: https://doi.org/10.1103/PhysRevB.37.785

[20] Krishnan, R., Binkley, J.S., Seeger, R., and Pople, J.A., "Self-consistent molecular orbital methods. XX. A basis set for correlated wave functions", The Journal of Chemical Physics, 72(1): 650-654, (1980), DOI: https://doi.org/10.1063/1.438955

[21] Dennington, R., Keith, T., and Millam, J., "GaussView, Version 5", Semichem Inc., Shawnee Mission KS, (2009).

[22] Niu, H.J., Mu, J.S., Zhang, M.L., Luo, J., Luo, P.H., Bai, X.D., and Wang, W., "Naphthalene-containing polyimides: Synthesis, characterization and photovoltaic properties of novel donor-acceptor dyes used in solar cell", Transactions of Nonferrous Metals Society of China, 19: 587-593, (2009). DOI: https://doi.org/10.1016/S1003-6326(10)60114-8

[23] Sen, A., and Groß, A., "Does involving additional linker always increase the efficiency of an organic dye for P-type dye-sensitized solar cells?", ACS Applied Energy Materials, 2(9): 6341-6347, (2019), DOI: https://doi.org/10.1021/acsaem.9b00973

[24] Spartan'14, Wavefunction Inc., 18401 Von Karman Avenue, Suite 370, Irvine, CA 92612, USA, (2014).

[25] Kucuk, C., Akdogan, N., Ozel, K., Erdogdu, Y., Disli, A., and Yildiz, A., "Structural, quantum chemical, spectroscopic (UV, FT-IR, and NMR), and molecular docking studies of novel azo compounds", Journal of Molecular Structure, 1319: 139318, (2024), DOI: https://doi.org/10.1016/j.molstruc.2024.139318.

[26] Soyarslan, K., Ortatepe, B., Yurduguzel, B., Güllüoğlu, M.T., and Erdogdu, Y., "An investigation into the structural, electronic, and non-linear optical properties in CN fullerene cages", Journal of Molecular Modeling, 28(11), (2022), DOI: https://doi.org/10.1007/s00894-022-05348-9

[27] Ozel, K., Atilgan, A., Akdogan, N., Yurdakul, E.B., Dilek, G., Yildiz, A., Disli, A., and Erdogdu, Y., "An assessment of the photovoltaic characteristics of some azo dyes for dye-sensitized solar cells: insights from experimental and theoretical studies", Optical and Quantum Electronics, 57(8), (2025), DOI: https://doi.org/10.1007/s11082-025-08359-x